Up-Conversion Luminescent and Porous $NaYF_4:Yb^{3+}$, $Er^{3+}@SiO_2$ Nanocomposite Fibers for Anti-Cancer Drug Delivery and Cell Imaging

Zhiyao Hou, Chunxia Li, Ping'an Ma, Ziyong Cheng, Xuejiao Li, Xiao Zhang, Yunlu Dai, Dongmei Yang, Hongzhou Lian, and Jun Lin**

Up-conversion (UC) luminescent and porous $NaYF_4:Yb^{3+}$, $Er^{3+}@SiO_2$ nanocomposite fibers are prepared by electrospinning process. The biocompatibility test on L929 fibrolast cells reveals low cytotoxicity of the fibers. The obtained fibers can be used as anti-cancer drug delivery host carriers for investigation of the drug storage/release properties. Doxorubicin hydrochloride (DOX), a typical anticancer drug, is introduced into $NaYF_4:Yb^{3+}$, $Er^{3+}@SiO_2$ nanocomposite fibers (denoted as DOX-$NaYF_4:Yb^{3+}$, $Er^{3+}@SiO_2$). The release properties of the drug carrier system are examined and the in vitro cytotoxicity and cell uptake behavior of these $NaYF_4:Yb^{3+}$, $Er^{3+}@SiO_2$ for HeLa cells are evaluated. The release of DOX from $NaYF_4:Yb^{3+}$, $Er^{3+}@SiO_2$ exhibits sustained, pH-sensitive release patterns and the DOX-$NaYF_4:Yb^{3+}$, $Er^{3+}@SiO_2$ show similar cytotoxicity as the free DOX on HeLa cells. Confocal microscopy observations show that the composites can be effectively taken up by HeLa cells. Furthermore, the fibers show near-infrared UC luminescence and are successfully applied in bioimaging of HeLa cells. The results indicate the promise of using $NaYF_4:Yb^{3+}$, $Er^{3+}@SiO_2$ nanocomposite fibers as multi-functional drug carriers for drug delivery and cell imaging.

1. Introduction

Silica-based materials, as an important family of inorganic biomaterials, have attracted much attention for their potential applications in biomedical and biotechnological fields due to their excellent biocompatibility, high surface areas with abundant Si–OH active bonds available for the loading of drug molecules, well-defined properties and diversity in surface functionalization.[1–15] Meanwhile, the development of multifunctional silica-based materials combining porous and luminescent properties in the drug delivery systems (DDSs) would meet the requirements of disease diagnosis and therapy, which show great potential applications in biomedical nanotechnology. The combination of porous and luminescence DDSs not only have high pore volumes for the storage and delivery of drugs but also possess luminescence properties which can be tracked to evaluate the efficiency of the drug release and can provide bi-functionalities of high sensitivity/resolution fluorescence imaging. Up to now, porous silica-based DDSs functionalized with luminescent property have potential applications in the fields of drug delivery, cell label and image, and disease diagnosis/therapy.[16–28]

Many biological samples (such as biological tissues in human body, fluorescent drug molecules) show auto-fluorescence under short-wavelength UV radiation, which greatly decrease the signal-to-noise and detection sensitivity. Compared with the down-conversion (DC) luminescent materials, the lanthanides based up-conversion (UC) luminescent materials can emit higher-energy visible photons after being excited by lower-energy near-infrared (NIR) photons.[29] Meanwhile, excitation with the NIR only results in a very weak auto-fluorescence background because the UV-excitable biological tissues and fluorescent drug molecules that interfered with normal phosphor luminescence can no longer be excited by NIR radiation.[30] In addition, NIR light with strong penetration ability is safe to the human body and less harmful to cells. Low detectable toxicity UC nanocrystals (NCs) are widely expected to be the most promising classes of luminescent probes, with high sensitivity and low background fluorescence.[31] Therefore, the design and development of the porous silica materials functionalized with UC luminescence property as drug carrier is undoubtedly of great importance in the field of drug delivery and cell imaging. Unfortunately, the general synthetic protocols to combine porous silica with diverse functional UC luminescent materials for various bio-applications are still lacking.[32–36]

Dr. Z. Hou, Dr. C. Li, Dr. P. Ma, Dr. Z. Cheng, Dr. X. Li, Dr. X. Zhang, Dr. Y. Dai, Dr. D. Yang, Dr. H. Lian, Prof. J. Lin
State Key Laboratory of Rare Earth Resource Utilization
Changchun Institute of Applied Chemistry
Chinese Academy of Sciences
Changchun 130022, P. R. China
E-mail: mapa675@ciac.jl.cn; jlin@ciac.jl.cn
Dr. Z. Hou
Key Laboratory of Superlight Materials and surface Technology
Ministry of Education
College of Materials Science and Chemical Engineering
Harbin Engineering University
Harbin 150001, P. R. China

DOI: 10.1002/adfm.201200082

The electrospinning technique has been developed since 1934 for the synthesis of one-dimensional (1D) nanomaterials.[37] Electrospinning is an effective and simple method for preparing nanofibers from a rich variety of materials,[38–47] such as polymers, inorganic and hybrid (organic-inorganic) compounds. Although some silica materials prepared by electrospinning have been reported,[48–56] to the best of our knowledge, few porous SiO_2 fibers functionalized with photoluminescence (PL) via electrospinning process have been really tested as drug storage/release systems to demonstrate their potential application. Recently, we have reported preparation of one-dimensional fiber-like porous silica materials owing self-activated DC and $NaYF_4$:Yb^{3+}, Er^{3+} decorated UC luminescent properties through electrospinning process, resulting in the formation of multifunctional materials, mainly focusing on the investigation of their luminescence and drug storage/release properties.[57,58] As a continuation of our former research, in this paper we intend to prepare multifunctional (porous structure and UC luminescence properties) $NaYF_4$:Yb^{3+}, Er^{3+} decorated SiO_2 nanocomposite fibers as anti-cancer drug carriers via the electrospinning method. Hydrophobic oleic acid capped cubic (α-) $NaYF_4$:Yb^{3+}, Er^{3+} nanocrystals (NCs) were transferred into aqueous phase by employing cetyltrimethylammonium bromide (CTAB) as a secondary surfactant. Then, the α-$NaYF_4$:Yb^{3+}, Er^{3+} NCs were dispersed into electrospinning precursor solution, followed by preparation of hybrid precursor fibers containing α-$NaYF_4$:Yb^{3+}, Er^{3+} NCs via electrospinning process. After annealing at 550 °C, porous SiO_2 nanocomposite fibers were obtained followed by a phase transition of the cubic (α-) $NaYF_4$:Yb^{3+}, Er^{3+} to the hexagonal (β-) $NaYF_4$:Yb^{3+}, Er^{3+} inside the SiO_2 fibers. The samples were fully characterized by means of XRD, SEM, TEM, N_2 adsorption and photoluminescence (PL) spectra, respectively. Doxorubicin hydrochloride (DOX) is one of the most widely used anti-cancer drugs due to its promising potential against solid tumors. The obtained materials have been studied as a DDS by using DOX as a model drug. The drug loading and release properties, cytotoxicity, and cellular uptake behavior were examined in detail. Furthermore, the effectiveness of $NaYF_4$:Yb^{3+}, Er^{3+}@SiO_2 nanocomposite fibers as a multifunctional fluorescent probe has been demonstrated by in vitro UC luminescence imaging.

2. Results and Discussion

2.1. Physical and Chemical Characterization of Nanocrystals and Composites

The physical and chemical properties of the obtained samples were characterized by means of XRD, SEM, TEM, UC emission spectra and N_2 adsorption/desorption analysis. Here we will present and analyze these results.

The as-synthesized α-$NaYF_4$:Yb^{3+}, Er^{3+} NCs are typically stabilized with hydrophobic oleic acid ligands and can be dispersed in nonpolar organic solvents. To conduct the electrospinning experiment to form porous SiO_2 fibers, it is necessary to transfer these hydrophobic ligand-capped NCs from organic phase to aqueous phase. Hyeon et al.[59] reported water-dispersible

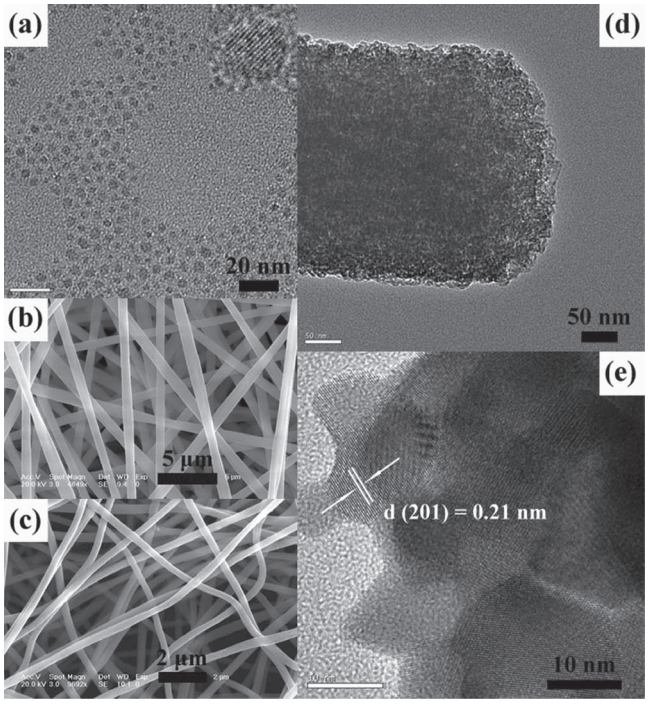

Figure 1. TEM image of water dispersed α-$NaYF_4$:Yb^{3+}, Er^{3+} NCs (a) with its HR-TEM image (inset), SEM images of the as-formed α-$NaYF_4$:Yb^{3+}, Er^{3+}@precursor fibers (b) and 550 °C annealing derived $NaYF_4$:Yb^{3+}, Er^{3+}@SiO_2 nanocomposite fibers (c), TEM (d) and HR-TEM (e) images of $NaYF_4$:Yb^{3+}, Er^{3+}@SiO_2 nanocomposite fibers.

Fe_3O_4 NCs prepared using CTAB. We used a similar approach to prepare water-dispersible α-$NaYF_4$:Yb^{3+}, Er^{3+} NCs by employing CTAB as a secondary surfactant. **Figure 1**a shows the TEM image, it can be clearly seen that α-$NaYF_4$:Yb^{3+}, Er^{3+} NCs dispersed in deionized water have good uniformity and monodispersity with an average diameter around 5 nm. After transferred to aqueous phase using CTAB, these NCs still preserve good monodispersity and very narrow size distribution. The corresponding HR-TEM (inset of Figure 1a) image shows clearly lattice fringes with interplanar spacing of 0.31 nm ascribed to (111) plane of α-$NaYF_4$. The UC emission spectrum of the as-synthesized α-$NaYF_4$:Yb^{3+}, Er^{3+} NCs are shown in Figure S1a (Supporting Information). In the emission spectrum for α-$NaYF_4$:Yb^{3+}, Er^{3+} NCs, the spectral peaks can be observed corresponding to the electron transitions of Er^{3+} ions: $^2H_{11/2}/^4S_{3/2} \rightarrow {}^4I_{15/2}$ (from 510 to 575 nm), $^4H_{9/2} \rightarrow {}^4I_{15/2}$ (660 and 675 nm),[60] the characteristic emission peaks are similar to those observed in previous study for the pure UC crystals.[61] Figure S1b (Supporting Information) gives the digital photograph of α-$NaYF_4$:Yb^{3+}, Er^{3+} NCs dispersed in deionized water, as well as the luminescent photograph under 980 nm NIR laser excitation (Figure S1c (Supporting Information)). The results demonstrate that the as synthesized α-$NaYF_4$:Yb^{3+}, Er^{3+} NCs can be well dispersed in above solution and emit red light. The triblock copolymers P123 is nonionic surfactant, which is composed of poly(ethylene oxide) (PEO) and poly(propylene oxide) (PPO). In dilute aqueous solutions, the PEO-PPO-PEO copolymers may self-assemble to form micelles, with a hydrophobic

core containing PPO, which is protected from the surrounding water by a water swollen PEO corona. Initially, P123 formed irregular micelles and rod-like micelles in ethanol solution containing TEOS and CTAB stabilized α-$NaYF_4$:Yb^{3+}, Er^{3+} NCs. Then PVP was added to adjust viscoelasticity of the solution, forming a hybrid sol for electrospinning. Micelles and CTAB stabilized α-$NaYF_4$:Yb^{3+}, Er^{3+} NCs can exist in the electrospinning precursor fibers. After being annealed at high temperature, porous SiO_2 fibers formed after removing PVP and P123 directing agent. Figure 1b and 1c show the SEM micrographs of as-prepared $NaYF_4$:Yb^{3+}, Er^{3+} decorated precursor fibers (labeled as α-$NaYF_4$:Yb^{3+}, Er^{3+}@precursor fibers) and those fibers annealed at 550 °C (labeled as $NaYF_4$:Yb^{3+}, Er^{3+}@SiO_2), respectively. It can be seen that the samples consist of uniform fibers with length of several tens to hundred micrometers. The as-formed precursor fibers are smooth with diameters ranging from 0.5 to 1.5 μm (Figure 1b). After being annealed at 550 °C, the fiber diameters decrease greatly to 150–500 nm due to the decomposition of the organic species inside the fibers (Figure 1c). The porous structure of SiO_2 fibers is further characterized by TEM technique. The typical TEM and HR-TEM images of $NaYF_4$:Yb^{3+}, Er^{3+}@SiO_2 annealed at 550 °C are shown in Figure 1d,e. From Figure 1d, it can be seen that the diameter of SiO_2 fibers is about 300 nm, which is well consistent with that observed from the SEM image (Figure 1c). The porous structure of SiO_2 fibers can be seen clearly from the high-magnification TEM image due to the different electron penetrability. Moreover, the obvious lattice fringes in the HR-TEM image (Figure 1e) confirm the high crystallinity of $NaYF_4$ NCs in the SiO_2 fibers after high temperature annealing. The distance of 0.21 nm between the adjacent lattice fringes of $NaYF_4$:Yb^{3+}, Er^{3+}@SiO_2 is well consistent with the d_{201} spacing of the hexagonal β-$NaYF_4$ (JCPDS No. 16–0334). The above possible formation process of the porous $NaYF_4$:Yb^{3+}, Er^{3+}@SiO_2 nanocomposite fibers is schematically shown in Figure S2 (Supporting Information).

Figure 2 shows the XRD patterns of the as-synthesized $NaYF_4$:Yb^{3+}, Er^{3+} NCs, the as-prepared $NaYF_4$:Yb^{3+}, Er^{3+}@

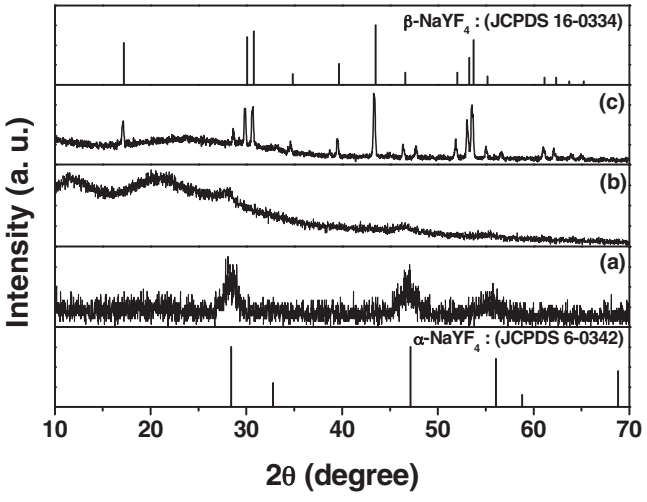

Figure 2. X-ray diffraction patterns for the as-synthesized α-$NaYF_4$:Yb^{3+}, Er^{3+} NCs (a), α-$NaYF_4$:Yb^{3+}, Er^{3+}@precursor fibers (b) and 550 °C annealing derived $NaYF_4$:Yb^{3+}, Er^{3+}@SiO_2 nanocomposite fibers (c).

precursor fibers and $NaYF_4$:Yb^{3+}, Er^{3+}@SiO_2 nanocomposite fibers, as well as the JCPDS cards for $NaYF_4$, respectively. In Figure 2a for $NaYF_4$:Yb^{3+}, Er^{3+} NCs obtained by thermal decomposition method, all the diffraction peaks for sample can be indexed as a pure cubic α-phase, which coincides well with the literature values (JCPDS No. 06–0342). Figure 2b shows the XRD pattern for the precursor fibers containing α-$NaYF_4$:Yb^{3+}, Er^{3+} NCs, in which the broad band is ascribed to the semi-crystalline PVP, and the other peaks can also be indexed to α-$NaYF_4$. When the precursor sample is calcined at 550 °C (Figure 2c), a broad peak centered at $2\theta = 22°$ can be observed due to the characteristic reflection from amorphous SiO_2 (JCPDS No. 29–0085), and α-phase $NaYF_4$ is drastically transformed to the β-phase (hexagonal) with the minor α-phase. The sharp diffraction peaks are in good agreement with the mixture of hexagonal β- phase and cubic α- phase structures known from bulk β- phase (JCPDS No. 06–0342) and α- phase (JCPDS No. 16–0334) $NaYF_4$. It is reported that the $\alpha \rightarrow \beta$ transition is exothermic, whereas $\beta \rightarrow \alpha$ is endothermic, indicating that the β-phase is a thermodynamically stable one.[62–64] The precursor of $NaYF_4$ prepared by a co-precipitation method, for instance, consisted of the α-phase, and then the annealing process at the high temperature caused the transition to β-phase. This phenomenon is attributed to the ordered-disordered arrangement of the cations.[63,64] In our preparation of $NaYF_4$:Yb^{3+}, Er^{3+}@SiO_2 nanoconposite fibers, the phase transformation of $NaYF_4$:Yb^{3+}, Er^{3+} from the cubic phase to the hexagonal phase with minor cubic phase occurs when the precursor fibers are annealed at 550 °C.

The respective N_2 adsorption/desorption isotherms of $NaYF_4$:Yb^{3+}, Er^{3+}@SiO_2 nanocomposite fibers and corresponding pore size distribution (inset) are shown in Figure S3 (Supporting Information). It can be seen that the SiO_2 samples show similar IV isotherms and the typical H_1-hysteresis loops, demonstrating the properties of a typical porous material. For the $NaYF_4$:Yb^{3+}, Er^{3+}@SiO_2, the BET surface area is about 260.67 m^2/g, pore volume is about 0.418 cm^3/g, and the pore size distribution shows a narrow apex centered at 6.41 nm. The uniform porous pore size (Figure S3 (Supporting Information), inset) is advantageous and favorable for the drug delivery applications. The UC emission spectrum and UC mechanisms of the as-prepared $NaYF_4$:Yb^{3+}, Er^{3+}@SiO_2 are shown in Figure S4 (Supporting Information), respectively. Under 980 nm NIR laser excitation, the UC emission spectrum of $NaYF_4$:Yb^{3+}, Er^{3+}@SiO_2 displays two typical emission bands upon excitation with a 980 nm laser diode: at 510–570 nm, attributable to the radiative transitions from $^4H_{11/2}/^4S_{3/2}$ to $^4I_{15/2}$, and at 630–700 nm from $^4F_{9/2}$ to $^4I_{15/2}$ of Er^{3+} (Figure S4a, (Supporting Information)). Up-conversion spectrum is subject to the surface properties of $NaYF_4$:Yb^{3+}, Er^{3+}, the presence of OH groups and photonic band gaps in the $NaYF_4$:Yb^{3+}, Er^{3+}@SiO_2 result in the quenching of green emission and enhancement of red emission.[65–67] Yan reported a novel UC photonic crystal fabricated by embedding $NaYF_4$:Yb^{3+}, Er^{3+} nanoparticles in inverse opals, and manipulates the UC emission behavior. A relatively intense red emission was observed, while the intensity of green emission decreased sharply.[66] The photonic band gap for the UC photonic crystal matches well with the green emission of $NaYF_4$:Yb^{3+}, Er^{3+}, and the luminescence spectrum

is affected by the 3D ordered structure and the green emission from $^4H_{11/2}/^4S_{3/2}$ to $^4I_{15/2}$ is suppressed significantly. The same reason may hold for the current $NaYF_4$:Yb^{3+}, Er^{3+}@SiO_2 fibers to some extent. The UC mechanisms in Yb^{3+}, Er^{3+} codoped materials are well investigated.[68,69] Initially, Yb^{3+} ions are excited from $^2F_{7/2}$ to $^2F_{5/2}$ level by 980 nm laser, and then an excited Yb^{3+} transfers its energy to Er^{3+} ($^4I_{11/2}$). Just as the electron stays on the $^4I_{11/2}$ level, a second 980 nm photon excites Yb^{3+} ions, and then the energy is transferred to Er^{3+}, resulting in the electron population on higher $^4F_{7/2}$ energetic state of the Er^{3+} ions. The Er^{3+} ion can then relax nonradiatively by a multiphonon relaxation process to the $^2H_{11/2}$ and $^4S_{3/2}$ levels and the dominant green $^2H_{11/2}\rightarrow{}^4I_{15/2}$ and $^4S_{3/2}\rightarrow{}^4I_{15/2}$ emissions occur. Alternatively, the electron can further relax and populate the $^4F_{9/2}$ level resulting in the occurrence of red $^4F_{9/2}\rightarrow{}^4I_{15/2}$ emission. The above excitation, energy transfer and up-conversion emission process is schematically shown in Figure S4b (Supporting Information).

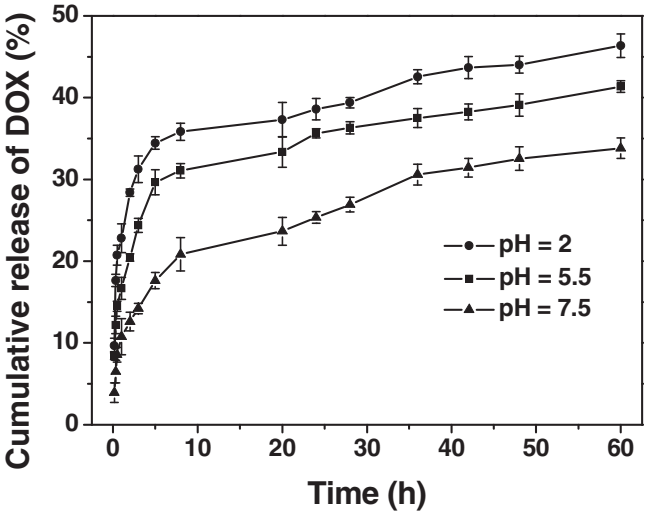

Figure 3. Drug release profiles for DOX-$NaYF_4$:Yb^{3+}, Er^{3+}@SiO_2 at pH = 7.5, 5.5 and 2 in PBS buffer.

2.2. The Biocompatibility of the $NaYF_4$:Yb^{3+}, Er^{3+}@SiO_2 Nanocomposite Fibers

The biocompatibility of the carrier materials would be key factor in evaluating the potential of DDSs. Only nontoxic carriers are suitable for drug delivery. It has been reported that the lanthanides based UC luminescent materials exhibit no or low cytotoxicity in vivo in some literatures.[70–73] The obtained $NaYF_4$:Yb^{3+}, Er^{3+}@SiO_2 nanocomposite fibers were incubated with L929 fibroblast cell, and MTT assay was used for the study on the cell viability of $NaYF_4$:Yb^{3+}, Er^{3+}@SiO_2. Cell viability is directly proportional to the amount of formazan produced monitored by the absorbance at 490 nm. The $NaYF_4$:Yb^{3+}, Er^{3+}@SiO_2 nanocomposite fibers were delivered over a range of dosages (1.5625–100 μg/mL). Figure S5 (Supporting Information) shows viability results, which indicate that more than 98% L929 fibroblast cells viability was observed under the varying concentration range, and showed satisfactory results that supported the biocompatibility of the porous fibers in all dosages. The result implies that the prepared $NaYF_4$:Yb^{3+}, Er^{3+}@SiO_2 nanocomposite fibers have good biocompatibility, which is an important prerequisite of the carriers for biomedical applications.

2.3. Drug Loading and Release Properties of $NaYF_4$:Yb^{3+}, Er^{3+}@SiO_2 Nanocomposite Fibers

Doxorubicin hydrochloride (DOX), an anti-cancer drug, was used as a model drug loaded into porous $NaYF_4$:Yb^{3+}, Er^{3+}@SiO_2 nanocomposite fibers, and the DOX release properties were examined. In our current DDS, the drug storage/release process was investigated according to the previous methods.[13,28,33] During the loading and release process, the DOX molecules can be adsorbed onto the surface of porous materials in the impregnation process and liberated by a diffusion-controlled mechanism.[13,28,33] The concentration of DOX in the DOX-$NaYF_4$:Yb^{3+}, Er^{3+}@SiO_2 could be calculated by $[(O_{DOX}\ R_{DOX})/O_{DOX}]\times100\%$, and the loading efficiency was 12.2 wt.% (O_{DOX} is the original DOX content, and R_{DOX} is the residual DOX content). The cumulative drug release profiles for the DOX-$NaYF_4$:Yb^{3+}, Er^{3+}@SiO_2 DDS as a function of release time in three different pH values phosphoric acidic buffer solutions (PBS) over a time period of 60 h at 37 °C are shown in **Figure 3**. In pH = 2.0 and 5.5 PBS, DOX showed faster release and the amount released from DOX-$NaYF_4$:Yb^{3+}, Er^{3+}@SiO_2 DDS reached 35% and 30% during the first 5 h, followed by gradual increase to 46% and 41% after 60 h. Meanwhile, the amount released was only 18% in the course of 5 h and then leveled off (34%) at pH = 7.5. Upon dialysis, approximately 31 wt.% of the drug was released within 42 h in pH = 7.5 PBS, whereas in the case of pH = 5.5 and 2.0 PBS it only took 8 h and 3 h to attain a comparable level of drug release. The drug release behavior shows that the liberation of DOX from $NaYF_4$:Yb^{3+}, Er^{3+}@SiO_2 is pH-dependent in the range between 2.0–7.5 (The release properties of DOX in high basic environment cannot be performed due to the change of DOX). This pH-sensitive DOX release behavior can be elucidated by the fact that the surface zeta-potential of the SiO_2 sample becomes more positive with the decrease of the pH value, and the weaken electrostatic adsorption force with positive charged DOX molecules results in the faster drug release.[74,75] Pure $NaYF_4$:Yb^{3+}, Er^{3+}@SiO_2 nanocomposite fibers showed negatively charged surfaces (–18.92 and –8.13 mv) and a change trend towards more positive with decreasing pH values (pH = 7.5 and 5.5). The zeta-potential of the nanocomposite fibers in pH = 2.0 PBS just reversed to be positive (+1.18 mv), which seted up an electrostatic repulsion with the positive charged DOX molecules. It is well known that the extracellular pH of many solid tumors is lower than normal tissues and presents an acidic microenvironment.[76,77] The pH-sensitive DOX release might be beneficial at the reduced pH values in intracellular lysosomes, endosomes and certain cancerous tissues for targeted release and controlled therapy at the pathological sites.[76,78]

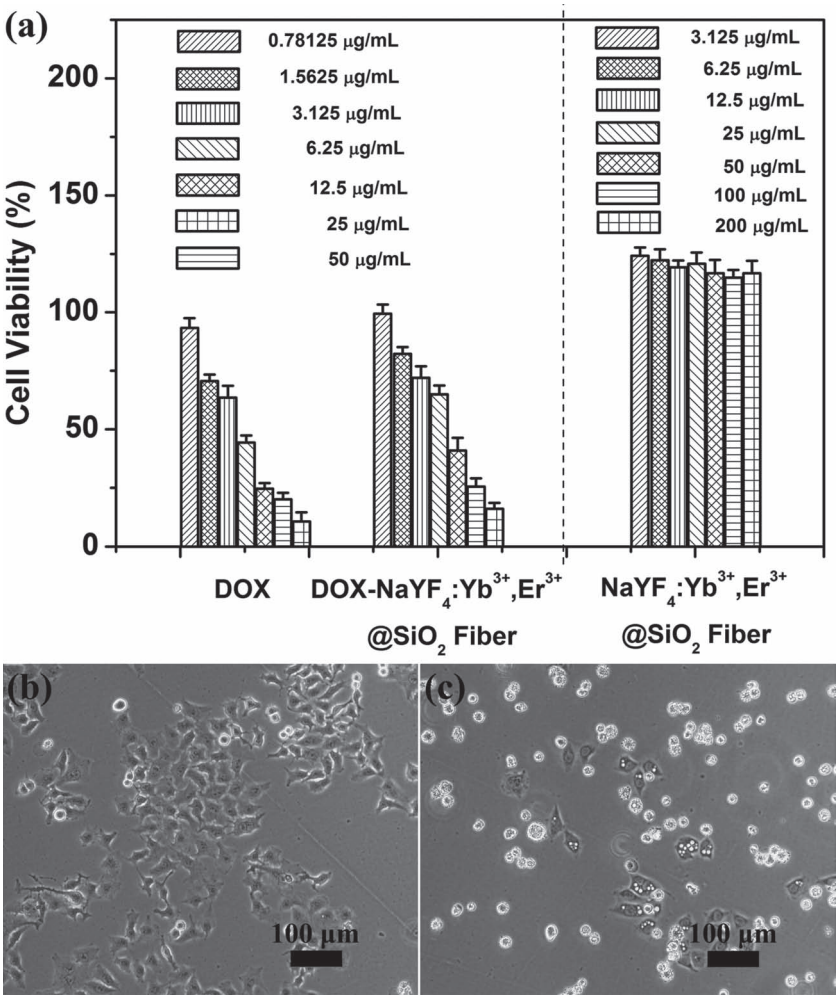

Figure 4. In vitro HeLa cell viabilities after incubation 24 h with free DOX, DOX-$NaYF_4$:Yb^{3+}, Er^{3+}@SiO_2 and pure $NaYF_4$:Yb^{3+}, Er^{3+}@SiO_2 at different concentrations (a). The nucleus of blank HeLa cells (b). The nucleus of HeLa cells incubated with DOX-$NaYF_4$:Yb^{3+}, Er^{3+}@SiO_2 for 24 h (c).

2.4. In Vitro Cytotoxicity Effect on Cancer and Normal Cells

To verify whether the released DOX was pharmacologically active, the cytotoxicity of the DOX-$NaYF_4$:Yb^{3+}, Er^{3+}@SiO_2 nanocomposite fibers on HeLa cells and L929 fibroblast cells are evaluated by MTT assay and the results were compared with free DOX and pure $NaYF_4$:Yb^{3+}, Er^{3+}@SiO_2. **Figure 4**a shows the cancer cell viabilities against free DOX, DOX-$NaYF_4$:Yb^{3+}, Er^{3+}@SiO_2, and $NaYF_4$:Yb^{3+}, Er^{3+}@SiO_2 for 24 h at different concentrations. The concentration of $NaYF_4$:Yb^{3+}, Er^{3+}@SiO_2 was set at the same level as the $NaYF_4$:Yb^{3+}, Er^{3+}@SiO_2 concentration used in the DOX-$NaYF_4$:Yb^{3+}, Er^{3+}@SiO_2. The pure $NaYF_4$:Yb^{3+}, Er^{3+}@SiO_2 without DOX has no adverse effect on cells viability within the tested concentration range, showing that $NaYF_4$:Yb^{3+}, Er^{3+}@SiO_2 itself has no obvious cytotoxic effect on HeLa cells. In contrast, the inhibitory concentration values for DOX and DOX-$NaYF_4$:Yb^{3+}, Er^{3+}@SiO_2 showed an increasing inhibition against HeLa cells with an increased concentration. It is found that the DOX-$NaYF_4$:Yb^{3+}, Er^{3+}@SiO_2 exhibits the similar cytotoxicity to that of free DOX. This may be attributed to the fact that the DOX-$NaYF_4$:Yb^{3+}, Er^{3+}@SiO_2 can be taken up by cell through endocytosis and release DOX inside to induce cell death. The IC_{50} values (the concentration of drug required to reduce cell growth by 50%) of DOX-$NaYF_4$:Yb^{3+}, Er^{3+}@SiO_2 and free DOX were 8.90 and 5.34 μg/mL, respectively. This may be significant because DOX-$NaYF_4$:Yb^{3+}, Er^{3+}@SiO_2 has comparable drug effect for inducing cancer cells death while the side effect of DOX was greatly abated due to the encapsulation of the drug inside the composites. The results indicate that the DOX-$NaYF_4$:Yb^{3+}, Er^{3+}@SiO_2 has a similar suppression effect on cancer cells in vitro compared with free DOX. Furthermore, compared with the HeLa cells nucleus (Figure 4b), the nuclei became fragmented (Figure 4c) after being treated with DOX-$NaYF_4$:Yb^{3+}, Er^{3+}@SiO_2. Figure S6 (Supporting Information) shows the L929 fibroblast cell (normal cell) viabilities against free DOX, DOX-$NaYF_4$:Yb^{3+}, Er^{3+}@SiO_2, and $NaYF_4$:Yb^{3+}, Er^{3+}@SiO_2 for 24 h at different concentrations. The DOX-$NaYF_4$:Yb^{3+}, Er^{3+}@SiO_2 exhibits the similar cytotoxicity to that of free DOX, and the viability of L929 fibroblast cells is higher than that of HeLa cells at high concentration of DOX. The results indicate that DOX-$NaYF_4$:Yb^{3+}, Er^{3+}@SiO_2 can not induce the extra effect to normal cells with respect to free DOX, and about 50% L929 fibroblast cells viability is observed under 50 μg/mL of DOX. Therefore, we conclude that $NaYF_4$:Yb^{3+}, Er^{3+}@SiO_2 nanocomposite fibers have potential to be used as a carrier for anti-cancer drugs.

2.5. Cellular Uptake and Biological Imaging of $NaYF_4$:Yb^{3+}, Er^{3+}@SiO_2 Nanocomposite Fibers

Porous $NaYF_4$:Yb^{3+}, Er^{3+}@SiO_2 nanocomposite fibers were ultrasonically treated before drug loading and cellular uptake, and the TEM image and dynamic light scattering data of fiber fragments are shown in Figure S7 (Supporting Information). From the TEM image (a), it can be seen that the length and diameter of fragments range from 350 nm to 1.25 μm and from 300 nm to 450 nm, respectively. The dynamic light scattering result is given in the Figure S7b (Supporting Information), which shows that the size of fiber fragments ranges from 90 nm to 3 μm (both length and diameter). Thus, we know that the ultrasonication can cut the long fibers (several hundred micrometers) into short ones effectively. The uptake and internalization of DOX-$NaYF_4$:Yb^{3+}, Er^{3+}@SiO_2 were investigated by confocal laser scanning microscope (CLSM) in HeLa cells incubated with DOX-$NaYF_4$:Yb^{3+}, Er^{3+}@SiO_2 ([DOX] = 20 μg/mL) for 10 min (a–c), 30 min (d–f), 1 h (g–i), and 6 h

(j–l) at 37 °C, respectively (Figure S8 (Supporting Information)). With increase of the incubation time, the intensities of red signal from DOX increase, that is, more DOX have crossed the membrane and localized in the cytoplasm. The red signal of DOX origins from DOX-composites or free DOX (DOX released from composites in medium) uptake by HeLa cells. Cellular uptake of $NaYF_4$:Yb^{3+}, Er^{3+}@SiO_2 was also determined using flow cytometry. The $NaYF_4$:Yb^{3+}, Er^{3+}@SiO_2 was labeled with FITC (fluorescent dye), and the cell uptake degree of the composite fibers could be quantified with flow cytometry by determining the green fluorescence emitted from FITC-$NaYF_4$:Yb^{3+}, Er^{3+}@SiO_2 treated HeLa cells. After incubation of HeLa cells with the sample for different times (10 min, 30 min, 1 h and 6 h), the cell-labeling ability of FITC-$NaYF_4$:Yb^{3+}, Er^{3+}@SiO_2 was estimated by flow cytometry. As revealed by **Figure 5**, FITC-$NaYF_4$:Yb^{3+}, Er^{3+}@SiO_2 nanocomposite fibers were taken up by HeLa cells compared to the controlled cells, and the cell uptake amount increases with incubation time. To further verify the location of the fibers relative to the HeLa cells, the CLSM photographs of HeLa cells incubated with FITC-labeled and DOX-loaded $NaYF_4$:Yb^{3+}, Er^{3+}@SiO_2 for 6 h are shown in **Figure 6**. The green fluorescence from the covalently linked FITC (λ_{ex} = 488 nm) and red fluorescence from DOX-$NaYF_4$:Yb^{3+}, Er^{3+}@SiO_2 (λ_{ex} = 575 nm) can be clearly seen in confocal images, demonstrating that the fiber fragments have been taken up by HeLa cells. The above results confirm that the $NaYF_4$:Yb^{3+}, Er^{3+}@SiO_2 nanocomposite fibers can be effectively taken up by HeLa cells. Thus, the effective therapy may result from the enhanced intracellular delivery, the pH-sensitive release and the protection of DOX extracellular by DOX-$NaYF_4$:Yb^{3+}, Er^{3+}@SiO_2.

By utilizing a modified inverted fluorescence microscopy equipped with infrared laser excitation at 980 nm, the interaction of HeLa cells with the $NaYF_4$:Yb^{3+}, Er^{3+}@SiO_2 nanocomposite fibers was also investigated by up-conversion luminescent microscopy (UCLM). HeLa cells were incubated with $NaYF_4$:Yb^{3+}, Er^{3+}@SiO_2 (100 μg/ml) at 37 °C for 4 h for cell imaging (**Figure 7**). Bright-field measurements after the treatment with $NaYF_4$:Yb^{3+}, Er^{3+}@SiO_2 confirmed that the cells are viable throughout the imaging experiments (Figure 7a). Moreover, an intense UC luminescence signal can be observed from the HeLa cells under laser excitation at 980 nm (Figure 7b). Overlays of bright-field and UC luminescent images further demonstrate that the luminescence is evident in the intracellular region (Figure 7c). This indicates that $NaYF_4$:Yb^{3+}, Er^{3+}@SiO_2 nanocomposite fibers penetrate the cell membrane of HeLa cells, agreeing well with the CLSM results. Thus, the result of UCLM confirms that $NaYF_4$:Yb^{3+}, Er^{3+}@SiO_2 nanocomposite fibers are promising candidates for use as bioimaging probes.

Cells use endocytosis for uptake of nutrients, down-regulation of growth factor receptors and as a master regulator of the signalling circuitry. There are several different types of endocytosis, all based on formation of intracellular vesicles following invagination of the plasma membrane or ruffling giving rise to larger vesicles. Phagocytosis (cell eating) is used for uptake of large particles, and is the first step in uptake and degradation of particles larger than 0.5 μm. Pinocytosis (cell drinking) is

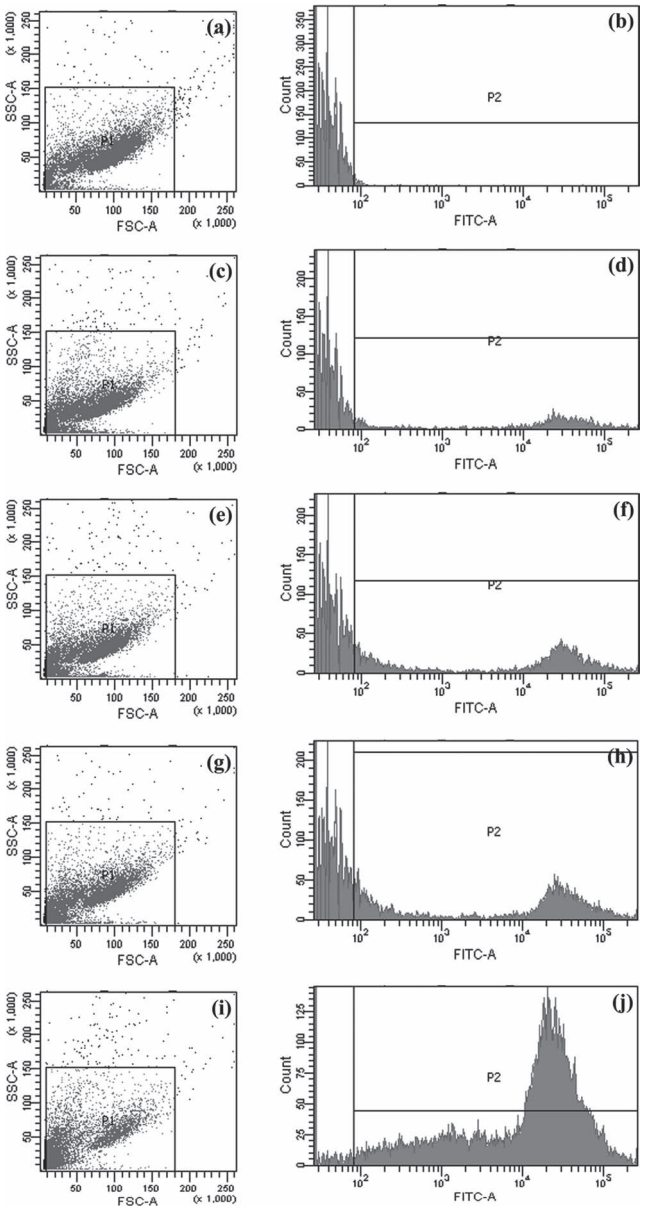

Figure 5. Flow cytometry analysis of the control cells (a,b) and HeLa cells incubated with FITC-$NaYF_4$:Yb^{3+}, Er^{3+}@SiO_2 for 10 min (c,d), 30 min (e,f), 1 h (g,h) and 6 h (i,j).

used to internalize fluid surrounding the cell, implying that all substances in the fluid phase area of invagination are taken up simultaneously. There are multiple types of endocytic pathways distinguished by specific molecular regulators. Nanoparticles and large particles taken up by endocytosis are enclosed within the early endosomes, phagosomes or macropinosomes.[79] After ultrasonically treating, the fragments of nanocomposite fibers belong to large particles, the fragments loading DOX taken up by endocytosis are enclosed within phagosomes, and then fuse with lysosomes. During the period of HeLa cells incubated with DOX-composites, DOX can be released from composites in the medium. These free DOX in the fluid phase area

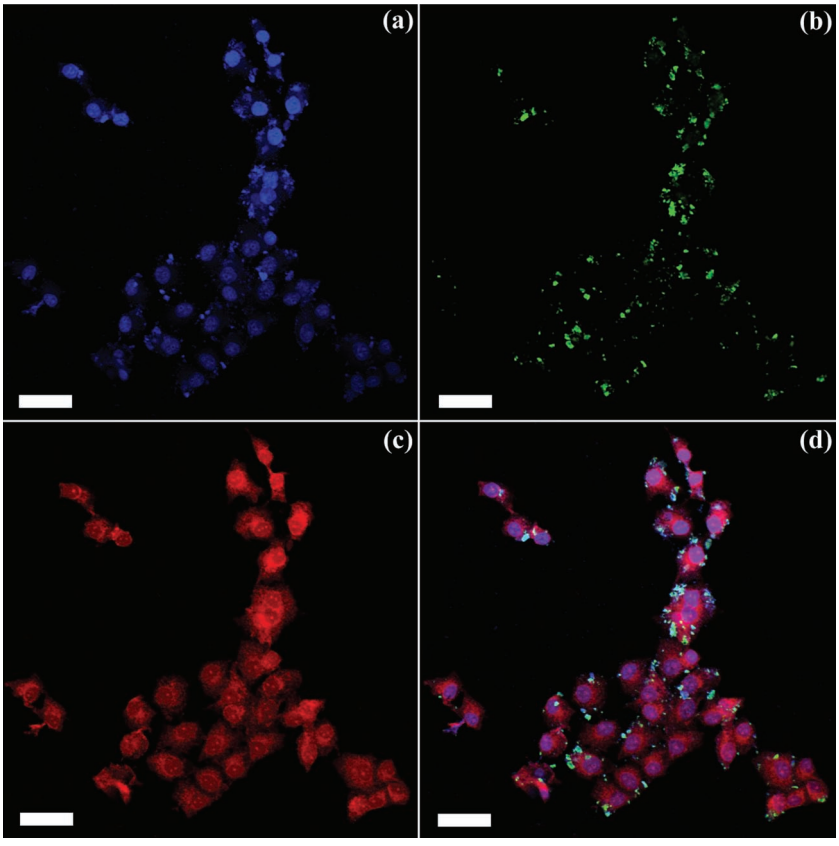

Figure 6. Confocal laser scanning microscopy (CLSM) images of HeLa cells incubated with FITC-labeled and DOX-loaded $NaYF_4$:Yb^{3+}, Er^{3+}@SiO_2 for 6 h. The images can be classified to the nuclei of cells (being dyed in blue by Hoechst 33324), FITC-labeled $NaYF_4$:Yb^{3+}, Er^{3+}@SiO_2, DOX-loaded $NaYF_4$:Yb^{3+}, Er^{3+}@SiO_2, and the merged images of all above, respectively. Scale bars for all images are 50 μm.

of invagination taken up by endocytosis are enclosed within the early endosomes, these vesicles with DOX then mature down the degradative pathway and become multivesicular bodies/late endosomes which fuse with lysosomes. Both endosomes (pH = 5.0–6.0) and lysosomes (pH = 4.0–5.0) have an acidic micro environment, which are distinct with the normal physiological environment (pH = 7.4). Compared with the normal tissues, solid tumors have a weakly acidic extracellular environment of pH < 7 due to the hypoxia-induced coordinated upregulation of glycolysis. The $NaYF_4$:Yb^{3+}, Er^{3+}@SiO_2 nanocomposite fibers can release the anti-cancer drug to induce apoptosis in endosomes and lysosomes acidic micro environment after the DOX-composites are internalized by the cancer cells through the endocytosis process.

3. Conclusions

In summary, oil-dispersible α-$NaYF_4$:Yb^{3+}, Er^{3+} NCs were synthesized by thermal decomposition methodology and transferred to polar solvents-soluble using CTAB. α-$NaYF_4$:Yb^{3+}, Er^{3+}@precursor fibers were prepared with electrospinning process using precursor solution containing α-$NaYF_4$:Yb^{3+}, Er^{3+} NCs, and $NaYF_4$:Yb^{3+}, Er^{3+}@SiO_2 nanocomposite fibers were obtained after high temperature annealing (550°C). The as-prepared $NaYF_4$:Yb^{3+}, Er^{3+}@SiO_2 nanocomposite fibers show the attracting properties of regular fiber-like morphology, porous structure, good biocompatibility, and UC emission, which are suitable for anti-cancer drug (DOX) storage/release as a drug carrier. It is found that the liberation of DOX from $NaYF_4$:Yb^{3+}, Er^{3+}@SiO_2 are pH-sensitive release pattern. DOX is shuttled into cell by porous $NaYF_4$:Yb^{3+}, Er^{3+}@SiO_2 carriers and released inside cells after endocytosis, and the DOX-$NaYF_4$:Yb^{3+}, Er^{3+}@SiO_2 exhibits the similar cytotoxicity with free DOX. Moreover, UCLM images of $NaYF_4$:Yb^{3+}, Er^{3+}@SiO_2 uptake by cells shows bright NIR UC emission, making the $NaYF_4$:Yb^{3+}, Er^{3+}@SiO_2 promising candidates for use as bioimaging agents. Therefore, the porous $NaYF_4$:Yb^{3+}, Er^{3+}@SiO_2 nanocomposite fibers may find potential applications in the fields of anti-cancer drug storage and cell imaging.

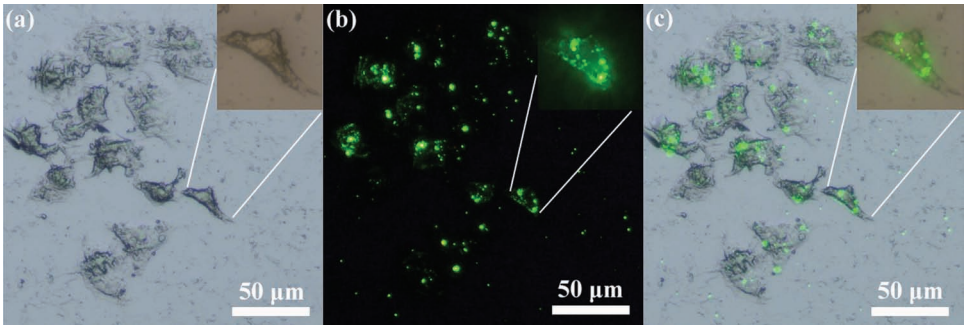

Figure 7. Inverted florescence microscope images of HeLa cells incubated with $NaYF_4$:Yb^{3+}, Er^{3+}@SiO_2 nanocomposite fibers, bright-field image (a), UC luminescent image (b) and the overlay of bright-field and UC luminescent images (c).

4. Experimental Section

Chemicals and Materials: Sodium oleate ($C_{15}H_{33}NaO_2$, chemically pure, C. P.) and n-hexane (C_6H_{14}, analytical reagent, A. R.) were purchased from Sinopharm Chemical Reagent Co., Ltd. Polyvinylpyrrolidone (PVP, M_w = 1,300,000), Oleic acid (OA), 1-Octadecene (ODE), aminopropyltrimethoxysilane (APTMS), $(EO)_{20}(PO)_{70}(EO)_{20}$ (P123, M_w = 5800) and Fluorescin isothiocyanate (FITC) were purchased from Aldrich. Trichloromethane ($CHCl_3$, A. R.) and Sodium fluoride (NaF, guaranteed reagent, G. R.) were purchased from Beijing Fine Chemical Company. Tetraethyl orthosilicate (TEOS, analytical reagent, A. R.) and Cetyltrimethylammonium bromide (CTAB, 99%) were purchased from Beijing Yili Fine Chemicals Co., Ltd. Doxorubicin hydrochloride (DOX) was purchased from Nanjing Duodian Chemical Regent Co., Ltd. All the initial chemicals in this work were used without further purification.

Synthesis of Water-Dispersible α-$NaYF_4$:Yb^{3+}, Er^{3+} NCs: *Synthesis of Rare Earth Oleate Complexes*: A literature method for the synthesis of iron-oleate complex[80] was adopted to prepare the rare earth oleate complexes. 10 mmol of rare earth chloride $RECl_3$ (RE = 80%Y + 17%Yb + 3%Er) and 30 mmol of sodium oleate were dissolved in a mixture solvent composed of 20 mL of ethanol, 15 mL of distilled water, and 35 mL of hexane. The resulting solution was added into a 250 mL round-bottomed flask with a reflux condenser, and then heated to 70 °C and kept at that temperature for 4 h. After the reaction was completed, the reaction mixture was transferred into a separatory funnel. The upper organic layer was separated and washed three times with 30 mL of distilled water. After being washed, rare earth oleate complexes were produced in a waxy solid form by evaporating off the remaining hexane.

Synthesis of Oleic Acid Stabilized α-$NaYF_4$:Yb^{3+}, Er^{3+} NCs: Oleic acid capped α-$NaYF_4$:Yb^{3+}, Er^{3+} NCs were synthesized by thermal decomposition methodology developed by Chen et. al.[62] In a typical procedure for the preparation of α-$NaYF_4$:Yb^{3+}, Er^{3+} NCs, 1 mmol of RE(oleate)$_3$ (RE = 80%Y+ 17%Yb + 3%Er), 12 mmol of NaF, 10 mL of OA and 10 mL of ODE were added to the three-neck round-bottom reaction vessel and subsequently heated to 120 °C under a vacuum with magnetic stirring for 30 min to remove residual water and oxygen, and flushed periodically with N_2. The reaction was kept at 280 °C for 0.75 h in N_2 atmosphere under vigorous stirring. When the reaction was completed, the transparent yellowish reaction mixture was allowed to cool to 80 °C, and the NCs were precipitated by the addition of ethanol and isolated via centrifugation. The finally obtained NCs could be readily dispersed in nonpolar solvents such as cyclohexane, toluene, and chloroform to form a colorless transparent colloid solution.

Transferring into Aqueous Phase of Oleic Acid Stabilized α-$NaYF_4$:Yb^{3+}, Er^{3+}: The synthesized oleic acid stabilized monodisperse NCs dispersed in 0.5 mL of chloroform was added to a 5 mL of aqueous solution containing 0.1 g CTAB. After vigorous stirring, the resulting solution was heated at 60 °C to induce evaporation of the chloroform of the solution, which generated aqueous-phase dispersed nanoparticles.[59]

Synthesis of UC Luminescent and Porous $NaYF_4$:Yb^{3+}, Er^{3+}@SiO_2 Nanocomposite Fibers: UC luminescence functionalized porous SiO_2 fibers were prepared by electrospinning process using P123 as structure directing agent and TEOS as silicon source. Typically, 0.25 g P123 was dissolved in 6.3 mL C_2H_5OH and 0.2 mL water soluble α-$NaYF_4$:Yb^{3+}, Er^{3+} NCs solution with magnetically stirring at room temperature for 0.5 h. Then 1mL TEOS was added dropwise to the solution with stirring at room temperature for 0.5 h. Finally, 0.59 g PVP was added to adjust the viscoelastic behavior of the solution. The solution was stirred for 3 h to obtain a homogeneous precursor sol for further electrospinning. The distance between the spinneret (a metallic needle) and collector (a grounded conductor) was fixed at 20 cm and the high-voltage supply was maintained at 10 kV. The spinning rate was controlled at 1.0 mL/h by a syringe pump (TJ-3A/W0109-1B, Baoding Longer Precision Pump Co., Ltd, China). The as-prepared hybrid precursor samples were annealed at 550 °C with the heating rate of 1 °C/min and held there for 3 h in air. Finally, $NaYF_4$:Yb^{3+},Er^{3+}@SiO_2 nanocomposite fibers were obtained. Porous $NaYF_4$:Yb^{3+}, Er^{3+}@SiO_2 were treated with ultrasonic before fluorescein label, drug loading and cellular uptake. FITC was labeled to $NaYF_4$:Yb^{3+}, Er^{3+}@SiO_2 as follows: 2 mg FITC and 45 µL APTMS were dissolved in 1 mL ethanol and stirred at room temperature for 12 h in the dark. Then 20 mg composites dispersed in 20 mL ethanol was added in 20 µL above solution and the mixture was refluxed at 80 °C for another 12 h. The composites were separated by centrifugation, washing with ethanol and dialysis against water (cutoff molecular weight: 8000–10000 Da).

The Biocompatibility of the $NaYF_4$:Yb^{3+}, Er^{3+}@SiO_2 Nanocomposite Fibers: To evaluate the biocompatibility of the $NaYF_4$:Yb^{3+}, Er^{3+}@SiO_2 nanocomposite fibers, MTT cell assay was used on the L929 cell. MTT is a standard test for screening the toxicity of biomaterials and is carried out in accordance with ASTM standards. Briefly, L929 fibroblast cells were plated out at a density of 5000–6000 cells per well in a 96 well plate and incubated overnight at 37 °C in a humidified atmosphere of 5% CO_2 to allow the cells to attach to the wells. The $NaYF_4$:Yb^{3+}, Er^{3+}@SiO_2 were sterilized by autoclaving, and then serial dilutions of the fibers at concentrations of 1.5625, 3.125, 6.25, 12.5, 25, 50 and 100 µg/mL were added to the culture wells to replace the original culture medium and incubated for another 24 h in 5% CO_2 at 37 °C. 5 mg/mL stock solution of MTT [3–(4,5–dimethylthiazol–2–yl)–2,5–diphenyltetrazolium bromide] was prepared in PBS and this stock solution (20 µL) was added to each well containing a different amount of the monodisperse $NaYF_4$:Yb^{3+}, Er^{3+}@SiO_2, and the plates were incubated at 37 °C for 4 h. The medium and MTT were then removed, and the MTT-formazan crystals were dissolved in 150 µL of DMSO, and place on a shaking table, 150 rpm for 5 minutes, to thoroughly mix the formazan into the solvent. The absorbance of the suspension was recorded under a microplate reader (Thermo Multiskan mk3) at 490 nm.

Preparation of Drug Storage/Delivery Systems: 10 mg of $NaYF_4$:Yb^{3+}, Er^{3+}@SiO_2 dispersing in 0.5 mL water was mixed with 4 mL of DOX aqueous solution (1 mg/mL). After stirred for 24 h under dark conditions, the DOX-loaded sample was collected by centrifugation and denoted as DOX-$NaYF_4$:Yb^{3+}, Er^{3+}@SiO_2. Then, DOX-$NaYF_4$:Yb^{3+}, Er^{3+}@SiO_2 were transferred to a dialysis tube and immersed in 2 mL pH = 7.5, 5.5 and 2 phosphoric acidic buffer solutions (PBS) at 37 °C with gentle shaking. At predetermined time intervals, PBS was taken by centrifugation and replaced with an equal volume of fresh PBS. The amounts of released DOX in the supernatant solutions were measured by UV-vis spectrophotometer at a wavelength of 480 nm. To evaluate the DOX-loading efficiency, the supernatant and washed solutions were collected and the residual DOX content (R_{DOX}) was obtained by UV-vis measurement at a wavelength of 480 nm. The loading efficiency of DOX can be calculated as follows: $[(O_{DOX}\ R_{DOX})/O_{DOX}]\times 100\%$, in which O_{DOX} is the original DOX content.

In Vitro Cytotoxicity of DOX-$NaYF_4$:Yb^{3+}, Er^{3+}@SiO_2 Against HeLa and L929 Cells: HeLa and L929 cells were plated out in 96-well plates at a density of 8000 cells per well and were allowed to attach and grow for 24 h to allow the cells to attach. The free DOX, DOX-$NaYF_4$:Yb^{3+}, Er^{3+}@SiO_2, and $NaYF_4$:Yb^{3+}, Er^{3+}@SiO_2 were added to the medium, and the cells were incubated in 5% CO_2 at 37 °C for 24 h. The concentrations of the fibers were 3.125, 6.25, 12.5, 25, 50, 100, 200 µg/mL, respectively. The concentrations of DOX were 0.78125, 1.5625, 3.125, 6.25, 12.5, 25, 50 µg/mL, respectively. At the end of the incubation, the media containing the nanocomposite fibers was removed, and 20 µL of MTT solution was added into each cell and incubated for another 4 h. The supernatant in each well was aspirated 150 µL of DMSO was added to each well before the plate was examined using a microplate reader (Therom Multiskan MK3) at the wavelength of 490 nm.

Cellular Uptake of the Porous $NaYF_4$:Yb^{3+}, Er^{3+}@SiO_2 Nanocomposite Fibers: Cellular uptake by HeLa cells was examined using flow cytometry and confocal laser scanning microscope (CLSM), respectively. For flow cytometry studies, HeLa cells (1×10^6) were seeded in 6-well culture plates and grown overnight. The cells were then treated with FITC-labeled $NaYF_4$:Yb^{3+}, Er^{3+}@SiO_2 at 37 °C for 10 min, 30 min, 1 h and 6 h. A single cell suspension was prepared consecutively by trypsinization, washing with PBS, and filtration through 35 mm nylon mesh. Thereafter, the cells were lifted using a cell stripper (Media Tech. Inc.), and analyzed using a FACSCalibur flow cytometer (BD Biosciences) for FITC. The

excitation wavelength and emission wavelength were 488 nm and 525 nm, respectively.

For CLSM, the HeLa cells were seeded in 6-well culture plates (a clean cover slip was put in each well) and grown overnight as a monolayer, and were incubated with DOX-$NaYF_4$:Yb^{3+}, Er^{3+}@SiO_2 at 37 °C for 10 min, 30 min, 1 h and 6 h (or FITC-labeled and DOX-loaded $NaYF_4$:Yb^{3+}, Er^{3+}@SiO_2 at 37 °C for 6 h). Thereafter, the cells were rinsed with PBS three times, fixed with 2.5% formaldehyde at 37 °C for 10 min, and then rinsed with PBS three times again. For nucleus labeling, fixed cells were incubated with Hoechst 33342 solution (from Molecular Probes, 20 mg/ml in PBS, 1 ml/well) for 10 min and then washed with PBS three times. The cover slips were placed on a glass microscope slide, and the samples were analyzed using CLSM for FITC and DOX.

UC Luminescent Imaging of the Porous $NaYF_4$:Yb^{3+}, Er^{3+}@SiO_2 Nanocomposite Fibers: The instrument of up-conversion luminescence microscopy (UCLM) was rebuilt on an inverted fluorescent microscope (Nikon Ti-S), an infrared laser excited unit (FF735-Di01-25 × 36, Nikon) and laser diode driver (KS3-11312-312, BWT). UC luminescence (UCL) bioimaging of HeLa (5×10^4/well) were seeded in 6-well culture plates (a clean cover slip was put in each well) and grown overnight as a monolayer, and were incubated with DOX-$NaYF_4$:Yb^{3+}, Er^{3+}@SiO_2 at 37 °C for 4 h. Thereafter, the cells were washed with PBS three times, fixed with 2.5% formaldehyde at 37 °C for 10 min, and then washed with PBS three times again. UCLM imaging was performed with the reconstructive Nikon Ti-S. Cells were excited by infrared laser at 980 nm (BWT Beijing LTD, China) with output power of 250 mW.

Characterization: The X-ray diffraction (XRD) patterns of the samples were carried out on a D8 Focus diffractometer (Bruker) with use of Cu Kα radiation (λ = 0.15405 nm). The UV–vis adsorption spectral values were measured on a U-3310 spectrophotometer. The morphology of the samples was inspected using a field emission scanning electron microscope (Philips XL 30). Transmission electron microscopy (TEM) micrograph was obtained from a FEI Tecnai G2 S-Twin transmission electron microscope with a field emission gun operating at 200 kV. Nitrogen adsorption/desorption analysis was measured using a Micromeritics ASAP 2020 M apparatus. The specific surface area was determined by the Brunauer–Emmett–Teller (BET) method using the data between 0.05 and 0.35. The pore volume was obtained from the t-plot method. The UC emission spectra were obtained using a 980 nm laser from an OPO (optical parametric oscillator, Continuum Sunlite, USA) as the excitation source and detected by a R955 (HAMAMATSU) from 400 to 700 nm. Confocal laser scanning microscopy (CLSM) images were observed by confocal laser scanning microscope (Olympus, FV 1000). The photos of up-conversion luminescence were obtained digitally on a Nikon multiple CCD camera (DS-Ri1). A flow cytometry (FCM, BD Biosciences) with an excitation wavelength of 488 nm was used to quantify the transfection efficiency of each sample.

Supporting Information

Supporting Information is available from the Wiley Online Library or from the author.

Acknowledgements

This project is financially supported by National Basic Research Program of China (2010CB327704), National High Technology Program of China (2011AA03A407), the National Natural Science Foundation of China (NSFC 20901074, 51172228, 21101149, 51172227, 20921002), the Postdoctoral Science Foundation of China (20100481070, 201104497), and Science and Technology Development Program of Jilin Province for Youths (20100106).

Received: January 11, 2012
Revised: February 24, 2012
Published online: April 13, 2012

[1] I. I. Slowing, B. G. Trewyn, S. Giri, V. S. Y. Lin, *Adv. Funct. Mater.* **2007**, *17*,1225–1236.
[2] J. H. Shin, S. K. Metzger, M. H. Schoenfisch, *J. Am. Chem. Soc.* **2007**, *129*, 4612–4619.
[3] E. M. Hetrick, J. H. Shin, N. A. Stasko, C. B. Johnson, D. A. Wespe, E. Holmuhamedov, M. H. Schoenfisch, *ACS Nano* **2008**, *2*, 235–246.
[4] T. Q. Nguyen, J. Wu, V. Doan, B. J. Schwartz, S. H. Tolbert, *Science* **2000**, *288*, 652–656.
[5] P. Kortesuo, M. Ahola, S. Karlsson, I. Kangasniemi, A. Yli-Urpo, J. Kiesvaara, *Biomaterials* **2000**, *21*, 193–198.
[6] W. Zhou, J. M. Thomas, D. S. Shephard, B. F. G. Johnson, D. Ozkaya, T. Maschmeyer, R. G. Bell, Q. F. Ge, *Science* **1998**, *280*, 705–708.
[7] C. Y. Lai, B. G. Trewyn, D. M. Jeftinija, K. Jeftinija, S. Xu, S. Jeftinija, *J. Am. Chem. Soc.* **2003**, *125*, 4451–4459.
[8] J. F. Chen, H. M. Ding, J. X. Wang, L. Shao, *Biomaterials* **2004**, *25*, 723–727.
[9] C. Barbé, J. Bartlett, L. Kong, K. Finnie, H. Q. Lin, M. Larkin, *Adv. Mater.* **2004**, *16*, 1949–1953.
[10] Y. F. Zhu, J. L. Shi, W. H. Shen, X. P. Dong, J. W. Feng, M. L. Ruan, *Angew. Chem. Int. Ed.* **2005**, *44*, 5083–5087.
[11] J. Andersson, J. Rosenholm, S. Areva, M. Lindén, *Chem. Mater.* **2004**, *16*, 4160–4167.
[12] Y. Chen, H. R. Chen, D. P. Zeng, Y. B. Tian, F. Chen, J. W. Feng, J. L. Shi, *ACS Nano* **2010**, *6*, 6001–6013.
[13] X. L. Huang, X. Teng, D. Chen, F. Q. Tang, J. Q. He, *Biomaterials* **2010**, *31*, 438–448.
[14] Q. J. He, J. L. Shi, F. Chen, M. Zhu, L. X. Zhang, *Biomaterials* **2010**, *31*, 3335–3346.
[15] R. Namgung, Y. Zhang, Q. L. Fang, K. Singha, H. J. Lee, I. K. Kwon, Y. Y. Jeong, I. K. Park, S. J. Son, W. J. Kim, *Biomaterials* **2011**, *32*, 3042–3052.
[16] J. W. Liu, A. S. Naughton, X. M. Jiang, C. J. Brinker, *J. Am. Chem. Soc.* **2009**, *131*, 1354–1355.
[17] S. L. Gai, P. P. Yang, C. X. Li, W. X. Wang, Y. L. Dai, N. Niu, J. Lin, *Adv. Funct. Mater.* **2010**, *20*, 1166–1172.
[18] J. W. Zhao, X. M. Liu, D. Cui, Y. J. Sun, Y. Yu, Y. F. Yang, C. Du, Y. Wang, K. Song, K. Liu, S. Z. Lu, X. G. Kong, H. Zhang, *Eur. J. Inorg. Chem.* **2010**, *12*, 1813–1819.
[19] L. N. Sun, H. J. Zhang, C. Y. Peng, J. B. Yu, Q. G. Meng, *J. Phys. Chem. B* **2006**, *110*, 7249–7258.
[20] J. Sauer, F. Marlow, B. Spliethoff, F. Schüth, *Chem. Mater.* **2002**, *14*, 217–724.
[21] L. M. Xiong, J. L. Shi, J. L. Gu, L. Li, W. M. Huang, J. H. Gao, M. L. Ruan, *J. Phys. Chem. B* **2005**, *109*, 731–735.
[22] P. P. Yang, Z. W. Quan, C. X. Li, X. J. Kang, H. Z. Lian, J. Lin, *Biomaterials* **2008**, *29*, 4341–4347.
[23] J. E. Lee, N. Lee, H. Kim, J. Kim, S. H. Choi, J. H. Kim, T. Kim, I. C. Song, S. P. Park, W. K. Moon, T. Hyeon, *J. Am. Chem. Soc.* **2010**, *132*, 552–557.
[24] M. Liong, J. Lu, M. Kovochich, T. Xia, S. G. Ruehm, A. E. Nel, F. Tamanoi, J. I. Zink, *ACS Nano* **2008**, *2*, 889–896.
[25] Y. Chen, H. R. Chen, S. J. Zhang, F. Chen, L. X. Zhang, J. M. Zhang, M. Zhu, H. X. Wu, L. M. Guo, J. W. Feng, J. L. Shi, *Adv. Funct. Mater.* **2011**, *21*, 270–278.
[26] L. Gu, J. H. Park, K. H. Duong, E. Ruoslahti, M. J. Sailor, *Small* **2010**, *6*, 2546–2552.
[27] P. Huang, Z. M. Li, J. Lin, D. P. Yang, G. Gao, C. Xu, L. Bao, C. L. Zhang, K. Wang, H. Song, H. Y. Hu, D. X. Cui, *Biomaterials* **2011**, *32*, 3447–3458.
[28] C. C. Huang, W. Huang, C. S. Yeh, *Biomaterials* **2011**, *32*, 556–564.
[29] a) M. Haase, H. Schäfer, *Angew. Chem. Int. Ed.* **2011**, *50*, 5808–5829; b) K. A. Abel, J. C. Boyer, F. C. J. M. van Veggel, *J. Am. Chem. Soc.* **2009**, *131*, 14644–14645; c) J. C. Boyer, L. A. Cuccia,

J. A. Capobianco, *Nano Lett.* **2007**, *7*, 847–852; d) N. M. Sangeetha, F. C. J. M. van Veggel, *J. Phys. Chem. C* **2009**, *113*, 14702–14707; e) P. Ghosh, J. Oliva, E. De la Rose, K. K. Halder, D. Solis, A. Patra, *J. Phys. Chem. C* **2008**, *112*, 9650–9658; f) H. Q. Wang, T. Nann, *ACS Nano* **2009**, *3*, 3804–3808; g) F. Wang, R. R. Deng, J. Wang, Q. X. Wang, Y. Han, H. M. Zhu, X. Y. Chen, X. G. Liu, *Nat. Mater.* **2011**, *10*, 968–973.

[30] a) L. Y. Wang, R. X. Yan, Z. Y. Hao, L. Wang, J. H. Zeng, J. Bao, X. Wang, Q. Peng, Y. D. Li, *Angew. Chem. Int. Ed.* **2005**, *44*, 6054–6057; b) F. Zhang, G. B. Braun, Y. F. Shi, Y. C. Zhang, X. H. Sun, N. O. Reich, D. Y. Zhao, G. Stucky, *J. Am. Chem. Soc.* **2010**, *132*, 2850–2851; c) B. M. van der Ende, L. Aarts, A. Meijerink, *Phys. Chem. Chem. Phys.* **2009**, *11*, 11081–11095; d) G. F. Wang, Q. Peng, Y. D. Li, *Acc. Chem. Res.* **2011**, *44*, 322–332; e) Z. H. Xu, P. A. Ma, C. X. Li, Z. Y. Hou, X. F. Zhai, S. S. Huang, J. Lin, *Biomaterials* **2011**, *32*, 4161–4173; f) F. Wang, X. G. Liu, *Chem. Soc. Rev.* **2009**, *38*, 976–989; g) J. Wang, F. Wang, C. Wang, Z. Liu, X. G. Liu, *Angew. Chem. Int. Ed.* **2011**, *50*, 10369–10372.

[31] a) H. Hu, M. X. Yu, F. Y. Li, Z. G. Chen, X. Gao, L. Q. Xiong, C. H. Huang, *Chem. Mater.* **2008**, *20*, 7003–7009; b) F. Wang, D. Banerjee, Y. S. Liu, X. Y. Chen, X. G. Liu, *Analyst* **2010**, *135*, 1839–1854; c) T. Y. Cao, Y. Yang, Y. Gao, J. Zhou, Z. Q. Li, F. Y. Li, *Biomaterials* **2011**, *32*, 2959–2968; d) Z. G. Chen, H. L. Chen, H. Hu, M. X. Yu, F. Y. Li, Q. Zhang, Z. G. Zhou, T. Yi, C. H. Huang, *J. Am. Chem. Soc.* **2008**, *130*, 3023–3029; e) J. Shen, L. D. Sun, C. H. Yan, *Dalton Trans.* **2008**, *42*, 5687–5697; f) M. Nyk, R. Kumar, T. Y. Ohulchanskyy, E. J. Bergey, P. N. Prasad, *Nano Lett.* **2008**, *8*, 3834–3838; g) D. T. Tu, L. Q. Liu, Q. Ju, Y. S. Liu, H. M. Zhu, R. F. Li, X. Y. Chen, *Angew. Chem. Int. Ed.* **2011**, *50*, 6306–6310; h) C. Wang, H. Q. Tao, L. Cheng, Z. Liu, *Biomaterials* **2011**, *32*, 6145–6154; i) Z. L. Wang, J. H. Hao, H. L. W. Chan, G. L. Law, W. T. Wang, K. L. Wong, M. B. Murphy, T. Su, Z. H. Zhang, S. Q. Zeng, *Nanoscale* **2011**, *3*, 2175–2181; j) Q. Li, Y. Sun, C. G. Li, J. Zhou, C. Y. Li, T. S. Yang, X. Z. Zhang, T. Yi, D. M. Wu, F. Y. Li, *ACS Nano* **2011**, *5*, 3146–3157; k) R. R. Deng, X. J. Xie, M. Vendrell, Y. T. Chang, X. G. Liu, *J. Am. Chem. Soc.* **2011**, *133*, 20168–20171.

[32] Y. F. Yang, Y. Q. Qu, J. W. Zhao, Q. H. Zeng, Y. Y. Ran, Q. B. Zhang, X. G. Kong, H. Zhang, *Eur. J. Inorg. Chem.* **2010**, *33*, 5195–5199.

[33] C. Wang, L. Cheng, Z. Liu, *Biomaterials* **2011**, *32*, 1110–1120.

[34] R. A. Jalil, Y. Zhang, *Biomaterials* **2008**, *29*, 4122–4128.

[35] N. M. Idris, Z. Q. Li, L. Ye, E. K. W. Sim, R. Mahendran, P. C. L. Ho, Y. Zhang, *Biomaterials* **2009**, *31*, 5104–5113.

[36] J. Zhou, Z. Liu, F. Y. Li, *Chem. Soc. Rev.* **2012**, *41*, 1323–1349.

[37] A. Formhals, US Patent **1934**, 1 975 504.

[38] S. Madhugiri, A. Dalton, J. Gutierrez, J. P. Ferraris, K. J. Balkus, *J. Am. Chem. Soc.* **2003**, *125*, 14531–14538.

[39] L. Yao, T. W. Haas, A. Guiseppi-Elie, G. L. Bowlin, D. G. Simpson, G. E. Wnek, *Chem. Mater.* **2003**, *15*, 1860–1864.

[40] G. Larsen, R. Velarde-Ortiz, K. Minchow, A. Barrero, I. G. Loscertales, *J. Am. Chem. Soc.* **2003**, *125*, 1154–1155.

[41] H. Yoshimoto, Y. M. Shin, H. Terai, J. P. Vacanti, *Biomaterials* **2003**, *24*, 2077–2082.

[42] H. Q. Hou, D. H. Reneker, *Adv. Mater.* **2004**, *16*, 69–73.

[43] J. Wu, J. L. Coffer, *Chem. Mater.* **2007**, *19*, 6266–6276.

[44] J. J. Ge, H. Hou, Q. Li, M. J. Graham, A. Greiner, D. H. Reneker, F. W. Harris, S. Z. D. Cheng, *J. Am. Chem. Soc.* **2004**, *126*, 15754–15761.

[45] M. J. Li, J. H. Zhang, H. Zhang, Y. F. Liu, C. L. Wang, X. Xu, Y. Tang, B. Yang, *Adv. Funct. Mater.* **2007**, *17*, 3650–3656.

[46] T. J. Sill, H. A. von Recum, *Biomaterials* **2008**, *29*, 1989–2006.

[47] J. S. Im, B. C. Bai, Y. S. Lee, *Biomaterials* **2010**, *31*, 1414–1419.

[48] S. S. Choi, S. G. Lee, S. S. Im, S. H. Kim, Y. L. Joo, *J. Mater. Sci. Lett.* **2003**, *22*, 891–893.

[49] S. S. Choi, B. Y. Chu, S. G. Lee, S. W. Lee, S. S. Im, S. H. Kim, J. K. Park, *J. Sol-Gel Sci. Technol.* **2004**, *30*, 215–221.

[50] A. C. Patel, S. X. Li, C. Wang, W. J. Zhang, Y. Wei, *Chem. Mater.* **2007**, *19*, 1231–1238.

[51] K. D. Min, J. H. Youk, Y. J. Kwark, W. H. Park, *Fibers Polym.* **2007**, *8*, 591–600.

[52] M. Krissanasaeranee, T. Vongsetskul, R. Rangkupan, P. Supaphol, S. Wongkasemjit, *J. Am. Ceram. Soc.* **2008**, *91*, 2830–2835.

[53] Y. Y. Zhao, H. Y. Wang, X. F. Lu, X. Li, Y. Yang, C. Wang, *Mater. Lett.* **2008**, *62*, 143–146.

[54] H. G. Kang, Y. H. Zhu, X. L. Yang, Y. J. Jing, A. Lengalova, C. Z. Li, *J. Colloid. Interface Sci.* **2010**, *341*, 303–310.

[55] Ki. Iimura, T. Oi, M. Suzuki, M. Hirota, *Adv. Powder Technol.* **2010**, *21*, 64–68.

[56] W. Wang, J. Y. Zhou, S. S. Zhang, J. Song, H. G. Duan, M. Zhou, C. S. Gong, Z. Bao, B. G. Lu, X. D. Li, W. Lan, E. Q. Xie, *J. Mater. Chem.* **2010**, *20*, 9068–9072.

[57] Z. Y. Hou, C. M. Zhang, C. X. Li, Z. H. Xu, Z. Y. Cheng, G. G. Li, W. X. Wang, C. Peng, J. Lin, *Chem. Eur. J.* **2010**, *16*, 14513–14519.

[58] Z. Y. Hou, C. X. Li, P. A. Ma, G. G. Li, Z. Y. Cheng, C. Peng, D. M. Yang, P. P. Yang, J. Lin, *Adv. Funct. Mater.* **2011**, *21*, 2356–2365.

[59] J. Kim, J. E. Lee, J. Lee, J. H. Yu, B. C. Kim, K. An, Y. Hwang, C. H. Shin, J. G. Park, J. Kim, T. Hyeon, *J. Am. Chem. Soc.* **2006**, *128*, 688–689.

[60] X. Wang, J. Zhuang, Q. Peng, Y. D. Li, *Nature* **2005**, *437*, 121–124.

[61] G. S. Yi, H. C. Lu, S. Y. Zhao, Y. Ge, W. J. Yang, D. P. Chen, L. H. Guo, *Nano Lett.* **2004**, *4*, 2191–2196.

[62] Y. Wei, F. Q. Lu, X. R. Zhang, D. P. Chen, *Chem. Mater.* **2006**, *18*, 5733–5737.

[63] J. S. Lee, Y. J. Kim, *Opt. Mater.* **2010**, *33*, 1111–1115.

[64] Y. Wei, F. Q. Lu, X. R. Zhang, D. P. Chen, *J. Alloys Compd.* **2007**, *427*, 333–340.

[65] Z. L. Wang, J. H. Hao, H. L. W. Chan, *J. Mater. Chem.* **2010**, *20*, 3178–3185.

[66] Z. X. Li, L. L. Li, H. P. Zhou, Q. Yuan, C. Chan, L. D. Sun, C. H. Yan, *Chem. Commun.* **2009**, *43*, 6616–6618.

[67] J. Pichaandi, F. C. J. M. van Veggel, M. Raundsepp, *ACS Applied Mater. Interface* **2010**, *2*, 157–164.

[68] S. Heer, K. Kompe, H. U. Gudel, M. Haase, *Adv. Mater.* **2004**, *16*, 2102–2105.

[69] J. F. Suyver, J. Grimm, K. W. Krämer, H. U. Güdel, *J. Lumin.* **2005**, *114*, 53–59.

[70] A. C. Ferrand, D. Imbert, A. S. Chauvin, C. D. B. van Dervyver, J. C. G. Büzli, *Chem. Eur. J.* **2007**, *13*, 8678–8687.

[71] L. Q. Xiong, Z. G. Chen, M. X. Yu, F. Y. Li, C. Liu, C. H. Huang, *Biomaterials* **2009**, *30*, 5592–5600.

[72] W. Wang, M. Zou, K. Chen, *Chem. Commun.* **2010**, *46*, 5100–5102.

[73] J. Zhou, Y. Sun, X. X. Du, L. Q. Xiong, H. Hu, F. Y. Li, *Biomaterials* **2010**, *31*, 3287–3295.

[74] S. H. Tang, X. Q. Huang, X. L. Chen, N. F. Zheng, *Adv. Funct. Mater.* **2010**, *20*, 2442–2447.

[75] M. Chen, S. X. Zhou, L. M. Wu, S. H. Xie, Y. Chen, *Macromol. Chem. Phys.* **2005**, *206*, 1896–1902.

[76] D. C. Drummond, M. Zignani, J. C. Leroux, *Prog. Lipid Res.* **2000**, *39*, 409–460.

[77] Z. M. Bhujwalla, D. Artemov, P. Ballesterors, S. Cerdan, R. J. Gillies, M. Solaiyappan, *NMR Biomed.* **2002**, *15*, 114–119.

[78] W. Wei, G. H. Ma, G. Hu, D. Yu, T. Mcleish, Z. G. Su, Z. Y. Shen, *J. Am. Chem. Soc.* **2008**, *130*, 15808–15810.

[79] T. G. Iversen, T. Skotland, K. Sandvig, *Nano Today* **2011**, *6*, 176–185.

[80] J. Park, K. J. An, Y. S. Hwang, J. G. Park, H. J. Noh, J. Y. Kim, J. H. Park, N. M. Hwang, T. Hyeon, *Nat. Mater.* **2004**, *3*, 891–895.